Use of Optical Coherent Detection for Environmental Sensing

Antonio Mecozzi, *Fellow, IEEE, Fellow, Optica*, Cristian Antonelli, *Senior Member, IEEE, Fellow, Optica*, Mikael Mazur, *Member, IEEE, Member, Optica*, Nicolas Fontaine, *Senior Member, IEEE, Fellow, Optica*, Haoshuo Chen, *Senior Member, IEEE, Member, Optica*, Lauren Dallachiesa, *Member, IEEE, Member, Optica*, and Roland Ryf, *Fellow, IEEE, Fellow, Optica*

(Invited Paper)

***Abstract*—We discuss the use of the fiber channel transfer matrix extracted from a digital coherent receiver for environmental sensing. We show that the polarization rotation vector describing the unitary part of the matrix is highly sensitive to perturbations affecting the optical fiber link. This vector can be readily extracted from the time-dependent transfer matrix reconstructed by the coherent receiver during system operation and may serve as an effective observable to monitor environmental changes.**

***Index Terms*—Polarization sensing.**

I. Introduction

THE cable of fiber optic coherent transmission systems is exposed to environmental perturbations, and the compensation of their effect requires that the receiver reconstructs the full transfer matrix of the link in real time. It has been recently shown [1], [2] that the analysis of the temporal evolution of the state of polarization obtained by applying the fiber transmission matrix to a *fixed* input state may reveal the nature of the perturbations that affect the cable, turning the latter into a distributed sensor. However, by looking only at the evolution of a fixed input state, as was done in [1], [2], some of the information contained in the fiber transfer matrix is lost.

In this work we discuss the use of various quantities that can be extracted from the measured transfer matrix, and compare their sensitivity to environmental perturbations. In particular, the matrix common phase is the most sensitive to time-dependent perturbations when the line-widths of the transmit and local oscillator lasers are sub-hertz. With telecommunication grade lasers, of line-width in the kilohertz or tens of kilohertz range, we find the rotation vector that characterizes the unitary part of the transfer matrix to be the most sensitive. This vector can be readily extracted from the transfer matrix reconstructed in real time by the digital coherent receiver during system operation and can be used as an effective observable to monitor environmental perturbations affecting the fiber link. Our observations are based on real-time data measured on cabled multi-core-fibers (MCF) with nominally uncoupled cores deployed in the city of L'Aquila, Italy [3]. The data were collected during a field trial in which a FPGA-based real-time transceiver has been operated continuously for approximately two months and the receiver readout stored for offline processing. Since we treated the DSP implemented by the transceiver as a black box, the data analysis imposed various practical challenges whose resolutions are also discussed in what follows.

The manuscripts covers and extends substantially the material presented in [4] and is organized as follows. Section II introduces the formalism and presents the analysis of the rotation vector (also supplemented with further detailed derivations in the appendix). Section III describes the procedure that allows to filter out slowly-varying changes in the rotation vector that are not induced by the perturbations of interest. Section IV is devoted to the analysis of the experimental data. Some conclusions are drawn in Section V.

Manuscript received 17 December 2022; revised 24 February 2023; accepted 1 March 2023. Date of publication 8 March 2023; date of current version 9 June 2023. The work of Antonio Mecozzi and Cristian Antonelli was supported in part by the Italian Government, in part by the project Innovating City Planning through Information and Communication Technologies (INCIPICT), and in part by the PRIN 2017 Project Fiber Infrastructure for Research on Space-Division Multiplexed Transmission (FIRST). *(Corresponding author: Antonio Mecozzi.)*

Antonio Mecozzi and Cristian Antonelli are with the Department of Physical and Chemical Sciences, University of L'Aquila, 67100 L'Aquila, Italy (e-mail: antonio.mecozzi@univaq.it; cristian.antonelli@univaq.it).

Mikael Mazur, Nicolas Fontaine, Haoshuo Chen, Lauren Dallachiesa, and Roland Ryf are with the Nokia Bell Labs, Murray Hill, NJ 07974 USA (e-mail: mikael.mazur@nokia-bell-labs.com; nicolas.fontaine@nokia-bell-labs.com; haoshuo.chen@nokia-bell-labs.com; lauren.dallachiesa@nokia-bell-labs.com; roland.ryf@nokia.com).

Color versions of one or more figures in this article are available at https://doi.org/10.1109/JLT.2023.3252444.

Digital Object Identifier 10.1109/JLT.2023.3252444

II. Analysis

We start by considering the polar decomposition of the matrix describing a single-mode fiber-optic link, which gives the channel matrix as the product of a unitary matrix and a positive semi-definite matrix, that is $\mathbf{T} = \mathbf{UA}$, where $\mathbf{U}$ is unitary, and $\mathbf{A}$ can be expressed as

$$\mathbf{A} = \left(\frac{g_0}{1+\gamma^2}\right)^{1/2} (\mathbf{I} + \vec{\gamma}\cdot\vec{\sigma})\,. \tag{1}$$

Here g_0 is the polarization-averaged intensity gain, $\vec{\gamma}$ is a three-dimensional real-valued vector with $\gamma = |\vec{\gamma}|$, and $\vec{\sigma} = \sigma_1\hat{e}_1 +$

$\sigma_2\hat{e}_2 + \sigma_3\hat{e}_3$ is the Pauli matrix vector [5], with

$$\sigma_1 = \begin{pmatrix} 1 & 0 \\ 0 & -1 \end{pmatrix}, \quad \sigma_2 = \begin{pmatrix} 0 & 1 \\ 1 & 0 \end{pmatrix}, \quad \sigma_3 = \begin{pmatrix} 0 & -i \\ i & 0 \end{pmatrix}. \tag{2}$$

The intensity transmission matrix $\mathbf{T}^\dagger\mathbf{T} = \mathbf{A}^\dagger\mathbf{A}$ can be written as

$$\mathbf{T}^\dagger\mathbf{T} = g_0(\mathbf{I} + \vec{\Gamma}\cdot\vec{\sigma}), \tag{3}$$

where $\vec{\Gamma} = 2\vec{\gamma}/(1+\gamma^2)$, is also a three-dimensional real-valued vector, known as the PDL vector [6]. The direction of $\vec{\Gamma}$ identifies the least and most attenuated polarization states in the Stokes space. It is customary to quantify the fiber-link PDL by means of the power ratio in dB between these states, which can be seen to be $\rho = 10\log[(1-\Gamma)/(1+\Gamma)]$, with $\Gamma = |\vec{\Gamma}|$ [6]. The unitary matrix $\mathbf{U}$ can be expressed as [5]

$$\mathbf{U} = \exp\left(-i\frac{\varphi_0}{2}\mathbf{I} - i\frac{\vec{\varphi}}{2}\cdot\vec{\sigma}\right), \tag{4}$$

with $\vec{\varphi} = \varphi\hat{\varphi}$, where $\hat{\varphi}$ is the three-dimensional unit vector that defines the polarization rotation axes in Stokes space and φ is the rotation angle of the field polarization from the input to the output. By φ_0 we denote the polarization-independent phase introduced by propagation. It should be noted that not only φ_0 is defined up to multiples of 2π, but also the expansion (4) is not unique, because of the identity $\mathbf{U} = (-1)^{m+n}\exp[-i(\varphi_0 + 2\,m\pi)\,\mathbf{I}/2 - i(\varphi + 2n\pi)\,\hat{\varphi}\cdot\vec{\sigma}/2]$, which holds for any pair of integers m and n. A change of sign of the Jones matrix does not affect the polarization state, so that besides the polarization averaged phase φ_0, also φ is defined up to multiples of 2π. The values of φ_0 and $\vec{\varphi}$ can be extracted from $\mathbf{U}$ through

$$\varphi_0 = i\,\mathrm{trace}\,[\log(\mathbf{U})] = i\log\,[\det(U)]\,, \tag{5}$$

$$\varphi_k = i\,\mathrm{trace}\,[\log(\mathbf{U})\,\sigma_k]\,, \quad k = 1,2,3, \tag{6}$$

where $-2\pi < \varphi_k < 2\pi$ if one uses the principal value of the logarithm matrix, that is, the logarithm with imaginary parts of the eigenvalues between $-\pi$ and π. This ensures that the length of $\vec{\varphi}$ is always less than 2π. Being $\vec{\varphi}$ equivalent to $\vec{\varphi}\,(1 - 2\pi/|\vec{\varphi}|)$, one may always restrict the length of the rotation vector between 0 to π by flipping its direction when its modulus exceeds π. Therefore in what follows we assume that this is always the case, namely $0 \le \varphi \le \pi$.

The coherent receiver provides an estimate of the inverse channel transmission matrix by attempting to equalize the received signal. We assume that the transmitted signal is polarization-multiplexed (PM), so that information is encoded in two independent signals transmitted over a pair of orthogonal polarization, say the x and y linear polarizations. After de-skew, orthonormalization, matched filtering, and dispersion compensation, the digitized samples are processed by the constant modulus algorithm (CMA). As is known, the CMA seeks a matrix $\mathbf{C}$ that, when applied to the received field, produces a constant-modulus output with a PM phase-modulated signal at the input [7] (QPSK in this work), or an output with a finite number of values of its modulus with a PM QAM-modulated signal at the input. This matrix is such that

$$\mathbf{CT} = \begin{pmatrix} e^{i\phi_1} & 0 \\ 0 & e^{i\phi_2} \end{pmatrix}, \tag{7}$$

where the phases ϕ_1 and ϕ_2 *add* to the actual phases of the *input* constellations $\phi_1^{(0)}$ and $\phi_2^{(0)}$ on the x and y polarization channels. With no loss of generality, in what follows we assume that the two constellations are synchronized so that the $\phi_1^{(0)} = \phi_2^{(0)} = 0$. Ideal channel reconstruction requires that also $\phi_1 = \phi_2 = 0$, so that $\mathbf{C}^{-1} = \mathbf{T}$. Rotations of the reconstructed constellations by ϕ_1 and ϕ_2, however, are unavoidable, as they are arise from a frequency mismatch between the transmit laser and the local oscillator, and do not affect the constant-modulus algorithm. They are extracted at a later stage, in the process of frequency estimation and phase estimation of the two polarization-multiplexed signals. The estimated transmission matrix $\mathbf{T}'$ is the inverse of the equalization matrix, $\mathbf{T}' = \mathbf{C}^{-1}$, and, using (7), it can be expressed as

$$\mathbf{T}' = \mathbf{T}\exp\left(-i\frac{\phi_1+\phi_2}{2}\mathbf{I} - i\frac{\phi_1-\phi_2}{2}\,\sigma_1\right). \tag{8}$$

In the absence of phase slips, we may assume that the error in the phase estimation is small and therefore that $|\phi_1 - \phi_2|$ is also small.

Defining the polar decomposition of the two transmission matrices as $\mathbf{T} = \mathbf{UA}$ and $\mathbf{T}' = \mathbf{U}'\mathbf{A}'$, it is possible to show that the unitary part $\mathbf{U}'$ of the polar decomposition of $\mathbf{T}'$ is related to the unitary part $\mathbf{U}$ of $\mathbf{T}$ via

$$\mathbf{U}' = \mathbf{U}\exp\left(-i\frac{\phi_1+\phi_2}{2}\mathbf{I} - i\frac{\phi_1-\phi_2}{2}\,\sigma_1\right). \tag{9}$$

This follows from noting that, denoting with $\mathbf{V}$ the second matrix on the right-hand side of (8), we have $\mathbf{T}' = \mathbf{TV} = (\mathbf{UA})\mathbf{V} = (\mathbf{UV})(\mathbf{V}^\dagger\mathbf{AV})$, so that $\mathbf{U}' = \mathbf{UV}$ and $\mathbf{A}' = \mathbf{V}^\dagger\mathbf{AV}$. In Stokes space the unitary matrices can be mapped into the link Mueller matrix $\mathbf{R}$ and its estimate matrices $\mathbf{R}'$, respectively, with

$$\mathbf{R} = \exp\,(\vec{\varphi}\times)\,, \tag{10}$$

$$\mathbf{R}' = \mathbf{R}\exp\,[(\phi_1 - \phi_2)\hat{e}_1\times]\,, \tag{11}$$

where by $\vec{\varphi}\times$ we denote a matrix that, when applied to a vector $\vec{s}$, yields the vector product $\vec{\varphi}\times\vec{s}$.

Equations (10) and (11) have an interesting geometrical interpretation in Stokes space, where the effect of a nonzero phase difference $\phi_1 - \phi_2$ is to add an undetermined rotation of the input polarization state around the axis $\hat{e}_1$. This rotation leaves the first component of the input signal Stokes vector unchanged, and therefore it does not affect the power in the x and y signal polarizations (the first component of the signal Stokes vector is defined as the power difference between the x and y signal polarizations, normalized to the total signal power). This fact has the obvious consequence that the CMA algorithm leaves $\phi_1 - \phi_2$ undetermined, and that only the x-polarized input state ($\hat{s} = \hat{e}_1$) and the y-polarized input state ($\hat{s} = -\hat{e}_1$) are not affected by the phase difference $\phi_1 - \phi_2$, being $\mathbf{R}'\hat{s} = \mathbf{R}\,\hat{s}$.

Expressing the matrix $\mathbf{U}'$ as

$$\mathbf{U}' = \exp\left(-i\frac{\varphi_0'}{2}\,\mathbf{I} - i\frac{\vec{\varphi}'}{2}\cdot\vec{\sigma}\right), \tag{12}$$

one can readily obtain the following simple relation between the actual and estimated phases

$$\varphi_0' = \varphi_0 + \phi_1 + \phi_2, \tag{13}$$

whereas a more cumbersome relation between the actual and estimated rotation vectors can be derived, as detailed in the Appendix. For small values of $\phi_1 - \phi_2$, as appropriate in the absence of phase slips, to first order in $\phi_1 - \phi_2$ the result is

$$\vec{\varphi}' = \vec{\varphi} + \vec{\kappa}(\vec{\varphi})(\phi_1 - \phi_2), \quad 0 \leqslant \varphi \leqslant \pi, \tag{14}$$

where we defined the coupling term

$$\vec{\kappa}(\vec{\varphi}) = \vec{\kappa}_1(\hat{\varphi}) + \left(\frac{\varphi}{2}\right)\vec{\kappa}_2(\hat{\varphi}) + \left(\frac{\varphi}{2}\right)\cot\left(\frac{\varphi}{2}\right)\vec{\kappa}_3(\hat{\varphi}), \tag{15}$$

with the mutually orthogonal set of vectors

$$\vec{\kappa}_1(\hat{\varphi}) = (\hat{\varphi}\cdot\hat{e}_1)\,\hat{\varphi}, \tag{16}$$

$$\vec{\kappa}_2(\hat{\varphi}) = \hat{\varphi}\times\hat{e}_1, \tag{17}$$

$$\vec{\kappa}_3(\hat{\varphi}) = \hat{\varphi}\times(\hat{e}_1\times\hat{\varphi}) = \hat{e}_1 - (\hat{\varphi}\cdot\hat{e}_1)\,\hat{\varphi}. \tag{18}$$

Equation (14) shows that the estimated rotation vector depends on the knowledge of the phase difference between the two constellations $\phi_1 - \phi_2$. Since we assumed that the two constellations are synchronized, ideally this difference would vanish, however this is not the case in practice, as the knowledge of ϕ_1 and ϕ_2 is affected by estimation errors due to the phase recovery algorithm. The length of the coupling vector $\kappa(\vec{\varphi})$ quantifies the strength of the dependence of the estimated rotation vector on the phase difference $\phi_1 - \phi_2$, is given by

$$|\vec{\kappa}(\vec{\varphi})|^2 = (\hat{\varphi}\cdot\hat{e}_1)^2 + \left[1 - (\hat{\varphi}\cdot\hat{e}_1)^2\right]\left(\frac{\varphi}{2}\right)^2\csc^2\left(\frac{\varphi}{2}\right), \tag{19}$$

and can be shown to range between 1 and $\pi/2$. The minimum length of 1 is attained either for $\varphi = 0$ and for any orientation of $\hat{\varphi}$, or for $\hat{\varphi} = \pm\hat{e}_1$ and for any value of φ. For a fixed orientation of $\hat{\varphi}$, the maximum length of the coupling vector is attained for $\varphi = \pi$, with an absolute maximum of $\pi/2$ for $\hat{\varphi}$ orthogonal to $\hat{e}_1$.

It is interesting to note that a non-zero coupling term converts a phase-mismatch between two constallations in the x and y polarizations into a polarization rotation, thereby enabling the receiver to phase-lock the two polarizations by the inversion of the channel's Jones matrix. In contrast, this effect may be detrimental for the purpose of monitoring the temporal changes of the rotation vector $\vec{\varphi}$, as is discussed in what follows.

We denote the fluctuations of the rotation vector by $\Delta\vec{\varphi}$. If these are small, to first order in $\phi_1 - \phi_2$ and $\Delta\vec{\varphi}$ the fluctuations of the estimated rotation vector can be expressed as

$$\Delta\vec{\varphi}' = \Delta\vec{\varphi} + \vec{\kappa}(\vec{\varphi})(\phi_1 - \phi_2). \tag{20}$$

This equation shows that only the component of $\Delta\vec{\varphi}'$ parallel to $\vec{\kappa}(\vec{\varphi})$ is affected by $\phi_1 - \phi_2$, whereas the component orthogonal to $\vec{\kappa}(\vec{\varphi})$ is not. If the time scale of the fluctuations of $\phi_1 - \phi_2$ is faster than the time scale of the fluctuations of $\Delta\vec{\varphi}$, and the compensation is wide-band, the phase recovery acts to lock this component to a constant value, thus canceling the fluctuations of the component of $\Delta\vec{\varphi}$ parallel to $\vec{\kappa}(\vec{\varphi})$ as well. If the fluctuations of $\phi_1 - \phi_2$ are slower than the fluctuations of $\Delta\vec{\varphi}$, and the compensation is narrow-band, then $\phi_1 - \phi_2$ can be considered as constant and $\Delta\vec{\varphi}'$ reproduces the fluctuations of $\Delta\vec{\varphi}$. Since the bandwidth of interest of the fluctuations of $\Delta\vec{\varphi}$ is in the hertz range, this is the case if $\phi_1 - \phi_2$ fluctuates over a similar time scale or more slowly. This requirements is of course fulfilled if the linewidths of the transmit laser and local oscillator are in the hertz or millihertz range.

It should be noted that the second term in (20) disappears altogether if phase recovery is performed jointly in the the two polarization channels. In this case the same phase fluctuations introduced by the transmit laser and the local oscillator affect the two polarization channels. Joint phase recovery, however, may require more advanced receiver schemes, of the kind used for high-dimensional modulation [8], with the result of decoupling the estimate of the channel's Jones matrix (and not only part of it) from the lasers' phase and frequency noise.

The considerations discussed above become more transparent in the relevant case of small φ and $\phi_1 - \phi_2$, where (20) becomes[1]

$$\Delta\vec{\varphi}' \simeq \Delta\vec{\varphi} + (\phi_1 - \phi_2)\,\hat{e}_1, \quad \varphi \ll \pi. \tag{21}$$

In this case, only the first component of $\vec{\varphi}'$ couples with $\phi_1 - \phi_2$, whereas the orthogonal components parallel to the second and third coordinate axes are uncoupled. The limit of small φ describes the case where the average polarization rotation is removed by numerical post compensation, as is discussed in what follows.

III. Compensated Mueller Matrix and Output Stokes Vectors

In this section we relate the fluctuations of the rotation vector with those of the field Stokes vector. To this end we start by removing the average polarization rotation. This can be done by numerically post-compensating for the average rotation vector $\langle\vec{\varphi}'\rangle$. Post-compensation is described by left multiplication of the Mueller matrix by $\exp(-\langle\vec{\varphi}'\rangle\times)$,

$$\mathbf{R}' = \exp\left(-\langle\vec{\varphi}'\rangle\times\right)\exp\left(\vec{\varphi}\times\right)\exp\left[(\phi_1 - \phi_2)\hat{e}_1\times\right] \tag{22}$$

The effect of this operation is to rotate the output Stokes vectors so that their center of mass on the Poincaré sphere coincides with the input Stokes vector. Note that, to avoid overburdening of the notation, we use the same symbols for the compensated Mueller matrix $\mathbf{R}'$ and rotation vector $\vec{\varphi}'$, and for the uncompensated quantities.

If the deviation of the output Stokes vectors from their average position is small, we may assume that the compensated rotation vector is also small, and expanding the exponential matrix to

[1]The same expression holds also for $\hat{\varphi} = \pm\hat{e}_1$, with no restrictions on the magnitude of ϕ.

first order therefore yields

$$\mathbf{R}' \simeq \mathbf{I} + \vec{\varphi}' \times = \begin{pmatrix} 1 & -\varphi_3' & \varphi_2' \\ \varphi_3' & 1 & -\varphi_1' \\ -\varphi_2' & \varphi_1' & 1 \end{pmatrix}, \qquad (23)$$

which shows that the three components of the rotation vector equal the off-diagonal terms $R_{i,j}$ of the compensated Mueller matrix $\mathbf{R}'$.

The fact that the components of the rotation vector of the compensated Mueller matrix are approximately equal to the non-diagonal matrix elements of $\mathbf{R}'$ gives a special meaning to this particular form of the rotation matrix. Indeed the matrix element $R_{i,j}$ represents the j-th component the output Stokes vector when the input is the i-th basis vector of Stokes space. In particular, for an x-polarized input state $\hat{s} = \hat{e}_1$, (23) yields

$$\mathbf{R}'\hat{e}_1 \simeq \hat{e}_1 + \vec{\varphi}' \times \hat{e}_1 = \hat{e}_1 + \varphi_3'\hat{e}_2 - \varphi_2'\hat{e}_3. \qquad (24)$$

On the other hand, (22) shows that for an x-polarized input, the output Stokes vector $\mathbf{R}'\hat{e}_1 = \exp(\langle\vec{\varphi}'\rangle\times)\exp(\vec{\varphi}\times)\hat{e}_1$ is independent of the phases ϕ_1 and ϕ_2, and hence (24) shows that the two components φ_2' and φ_3' of the rotation vector orthogonal to $\hat{e}_1$ are not affected by the relative orientations of the two constellations. This confirms the conclusion drawn from (21).

Note that the quantities φ_2' and φ_3' describe the cloud formed by the output Stokes vectors' tips around their distribution's center of mass with an x-polarized input. The instantaneous deviations of the output Stokes vectors from the center of mass corresponding to an x-polarized input were exactly the quantities measured in [1] and [2]. Therefore, the quantities measured in those papers were the components of the compensated rotation vectors independent of the relative orientations of the two constellations. This explains the high sensitivity of the measurements presented in [1], which were indeed obtained with a system in which transmit and local oscillator lasers had typical telecom-grade line-widths, in the tens of kilohertz range. The only component of the rotation vector left undetermined by a measurement of the output corresponding to an x-polarized input is that parallel to $\hat{e}_1$, namely φ_1', which is the only one sensitive on the relative orientations of the two constellations.

We conclude this section by noting that the characterization of environmental perturbations through the analysis of time changes of the channel transfer matrix is most effective when these depend linearly on the perturbations by which they are generated. This is because in this case the spectrum of the time-dependent fiber transfer matrix replicates the spectral features of the perturbations affecting the fiber, which allows to identify the nature of the perturbations by means of their spectral signature. In the presence of strong perturbations on which time changes of the fiber channel matrix depend nonlinearly, our analysis may still be useful, provided that the strong perturbations are characterized by a different timescale than the small perturbations and therefore they can be filtered out, e.g. by using moving-average techniques [1], [2]. This may be the case of aerial fiber cables, which are sometimes exposed to severe atmospheric conditions. In all cases, even in the presence of strong perturbations, polarization changes are expected to be always much slower than the update clock rate of the digital signal processing of the receiver (typically in the range of 100 MHz to 1 GHz).

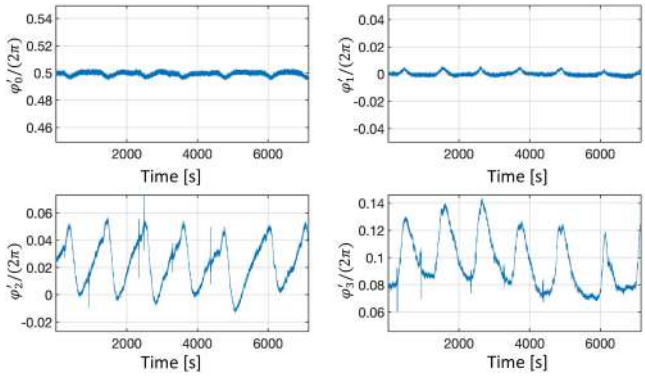

Fig. 1. Plot of the polarization-averaged phase $\varphi_0'/(2\pi)$ and of the three components of $\vec{\varphi}'/(2\pi)$ vs. time.

IV. Experimental Results

The experimental values of $\mathbf{T}'$ were measured in a recent real-time field trial [9] by concatenating the cores of a 6.3-km-long uncoupled-core 4-core fiber deployed in the city of L'Aquila, Italy [3], so as to form a link of 25.2 km. The DSP of the receiver was based on a mean-square error estimation scheme, and was operating at a frequency $f_0 = 125$ MHz, with a baud rate $R = 1$ GBd (see [9] for a detailed description of the experimental setup). The transmit and LO oscillator lasers were external cavity lasers with a line-width of 30 kHz. The parameters of $\mathbf{T}'$ were extracted with a downsampling factor (including low-pass filtering) of 2^{16} and hence the effective sampling period was $2^{16}/f_0 \simeq 524\,\mu$s. After extracting the unitary part $\mathbf{U}'$ by singular value decomposition, we have used (5) and (6) to obtain the polarization-averaged phase φ_0' and the components of the rotation vector $\vec{\varphi}'$.

Fig. 1 shows the three components of $\vec{\varphi}'$ and the phase φ_0' versus time during a two-hour data acquisition. Like in all the subsequent figures, the sampling rate has been reduced by a factor 1000 from the original value by filtering and decimation. First of all, by inspection of the three components of $\vec{\varphi}$ it can be seen that in the selected time window the modulus of the rotation vector is small, in the range of validity of (21). The figure also shows a similarity between φ_1' and φ_0', which indicates that they are contributed mainly by ϕ_1 and ϕ_2, consistently with (13) and (21), thereby preventing the extraction of φ_0 and φ_1. This implies that only two (out of four) parameters that are necessary to extract $\mathbf{U}$ are immune to the fluctuations of ϕ_1 and ϕ_2. The second and third components of $\vec{\varphi}'$ in Fig. 1 show temporal fluctuations with a period of approximately 20 minute reflecting the time dynamics of the air conditioning system in the laboratory. The most interesting features of these curves are however small perturbations that most likely are caused by events related to construction works taking place in the downtown area of l'Aquila, along the fiber route. These perturbations are absent in the first component of $\vec{\varphi}'$ and in the polarization-averaged phase φ_0', which are indeed much more

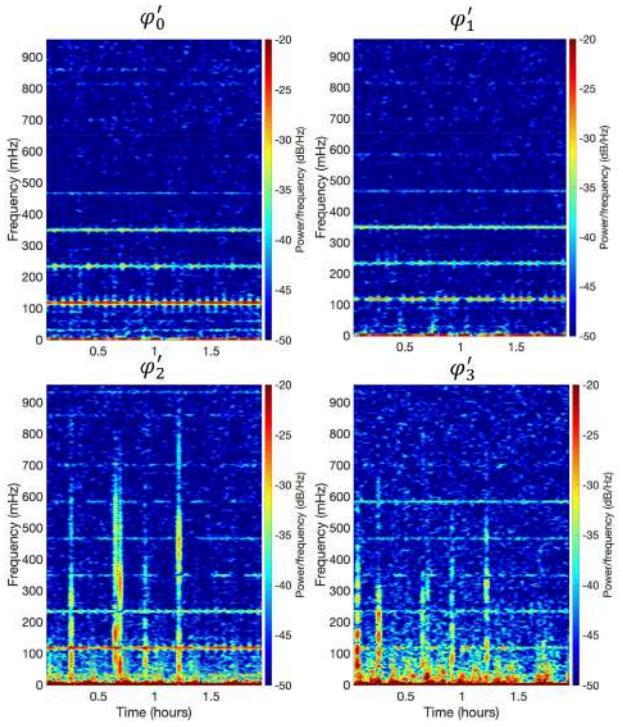

Fig. 2. Spectrograms of the polarization-averaged phase φ'_0 and of the three components of $\vec{\varphi}'$.

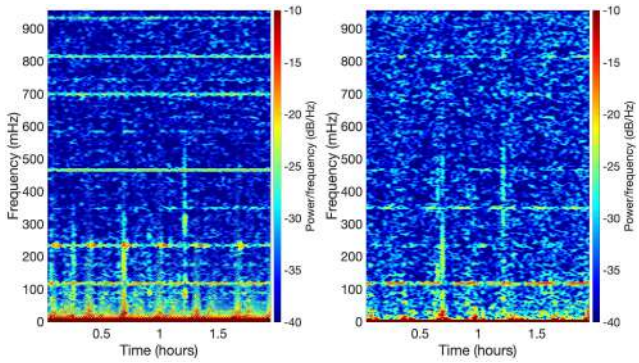

Fig. 3. Left panel, spectrogram of the polarization averaged gain. Right panel, spectrogram of the PDL in dB.

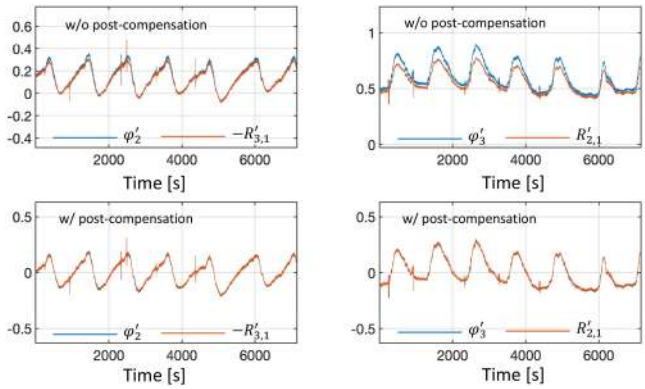

Fig. 4. The top panels show the temporal traces of φ_2 and $-R'_{3,1}$ (left), and of φ_3 and $R'_{2,1}$ (right). The elements of $\mathbf{R}'$ are plotted in red, while the components of $\vec{\varphi}'$ are plotted in blue. The lower panels show a plot of the same quantities, after compensation of the average rotation (as discussed in Section III).

stable. These features are confirmed by the spectrograms shown in Figs. 2. The vertical stripes in the spectrograms of φ'_2 and φ'_3 correspond to the perturbations that appear in the corresponding temporal traces, and are absent in the spectrograms of φ'_0 and φ'_1.

The fact that both φ'_0 and φ'_1 are not sensitive to the perturbations occurring along the fiber route can be explained by noting that these perturbations produce time-dependent changes in φ'_0 and $\vec{\varphi}'$ of (13) and (21). However, the frequency and phase estimation algorithms have no way to discriminate between the frequency and phase fluctuations caused by φ_0 and $\vec{\varphi}$ from those arising from the frequency mismatch and the phase diffusion of the two lasers. Therefore, the fluctuations due to environmental disturbances are compensated too, and this explains why the time traces of φ'_0 and φ'_1 do not record these fluctuations, but rather the result of the frequency and phase recovery algorithm trying to keep the phase of the two channels locked. The components φ'_2 and φ'_3 are not affected by the frequency and phase recovery algorithm and therefore they are sensitive to environmental perturbations.

Fig. 1 shows also horizontal lines at frequencies that are multiples of $f = 117.5$ mHz. These are determined by the periodicity of the pseudo-random bit sequences (PRBSs) used in the measurement and the DSP readout frequency. In this experiment, a PRBS with $(2^{23} - 1)$ bits was used for the load and an independent PRBS with $(2^7 - 1)$ bits was used for the header. With the baud rate $R = 1$ GBd used in the field trial, the modulated signal was periodic with period $T_R = N_p/R$ with $N_p = (2^{23} - 1)(2^7 - 1)$ (independent of the number of bits per symbol of the transmitted QAM constellations, as a result of the fact that N_p is an odd number hence not a multiple of any power of 2). The DSP readout frequency $f_0 = 125$ MHz was 8 times smaller than R, and therefore, being N_p not a multiple of 8, the *sampled* received signal was periodic with a period 8 times larger, $T_s = N_p/f_0$. This is consistent with the appearance of resonances at $f' = f_0/N_p = 117.3$ mHz. Being the observation window $T \simeq 7148$ s, $f' \simeq f$ within the temporal resolution of the measurement, $1/T \simeq 0.14$ mHz.

Vertical stripes and horizontal lines appear also in the spectrograms of the polarization-averaged gain and of the PDL in dB shown in Fig. 3. This is because in a fiber with random birefringence the polarization-averaged gain and PDL are coupled to polarization if the PDL is distributed along the line [10], and hence gain and PDL are expected to show similar spectral features as polarization. In Fig. 4 we test the accuracy of the approximated relation between $\mathbf{R}'$ and $\vec{\varphi}'$ in (23). The top panels show traces of $R'_{2,1}$ and φ'_3 (left), and of $R'_{1,3}$ and φ'_2 (right), in the same time interval as in Fig. 1. The elements of $\mathbf{R}'$ are plotted in red, while the components of $\vec{\varphi}'$ are plotted in blue. The good agreement between the two quantities is an indication of the accuracy of (23). The lower panels show the same traces, after compensation of the average rotation (as discussed in Section III). In this case the difference between the matrix elements and the components of the rotation vector practically disappears.

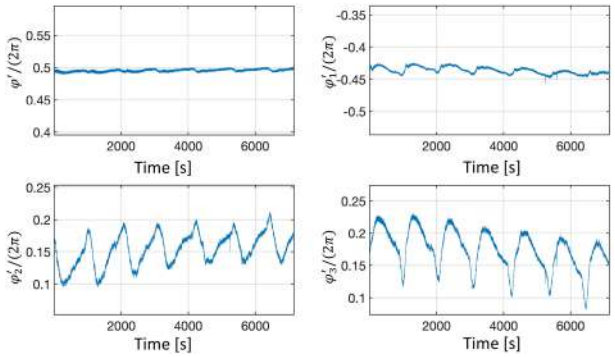

Fig. 5. Plot of the three components of the vector $\vec{\varphi}'/(2\pi)$ and of its modulus $\varphi'/(2\pi)$ versus time. The sampling rate has been reduced by a factor 1000 from the original value by filtering and decimation. The modulus of the rotation vector here is of the order of π, in contrast to the case of Fig. 1, where is was much smaller.

We note that the rotation vector analyzed in this section was small per se, as no post-compensation was implemented. This is not the case in other data sets, as is illustrated in the remainder of this section.

Fig. 5 shows a plot of the three components of $\vec{\varphi}'/(2\pi)$ and of its modulus $\varphi/(2\pi)$ versus time in a two-hour time interval where the modulus of the rotation vector is never small. In this case, (20) dictates that the noise of $\phi_1 - \phi_2$ couples to all the components of the rotation vector $\vec{\varphi}$. This is confirmed by the spectrograms of the three components of the rotation vector, which are plotted together with the spectrogram of the polarization-averaged phase in Fig. 6. The first manifestation of the mixing is that all three components are sensitive to two events, characterized by a wide-band excitation, that occurred during the two-hour time interval and are absent in the spectrogram of the phase. In this particular data set, $\varphi' \simeq \varphi \simeq \pi$ and hence (20) becomes

$$\Delta\vec{\varphi}' \simeq \Delta\vec{\varphi} + [(\hat{\varphi}\cdot\hat{e}_1)\,\hat{\varphi} + (\vec{\varphi}/2)\times\hat{e}_1]\,(\phi_1 - \phi_2), \quad \varphi \simeq \pi. \tag{25}$$

This equation shows that all components are directly affected by the laser phase noise, and that their coupling to phase noise is mediated by $\hat{\varphi}$, which is also a fluctuating quantity. Since the bandwidth of the product of two fluctuating quantities equals the sum of the bandwidths of each term, and the fluctuations are larger for the second and third components, this explains the broadband noise observed in the spectrograms of φ'_2 and φ'_3. The coupling disappears when the mean rotation vector is removed by post-compensation. This can be seen in the spectrograms shown in Fig. 7. Interestingly, the broad-band noise in the two components φ'_2 and φ'_3 that that is present in Fig. 6 also disappears, which is the consequence of the decoupling of these two components from the phase and frequency noise of the transmit and local oscillator implied by (21). This result shows that, after post-compensation, the component of the measured rotation vector $\vec{\varphi}'$ parallel to $\hat{e}_1$ is always insensitive to environmental perturbations affecting the same component of actual rotation vector $\vec{\varphi}$. Finally, Fig. 8 shows a scatter plot of the

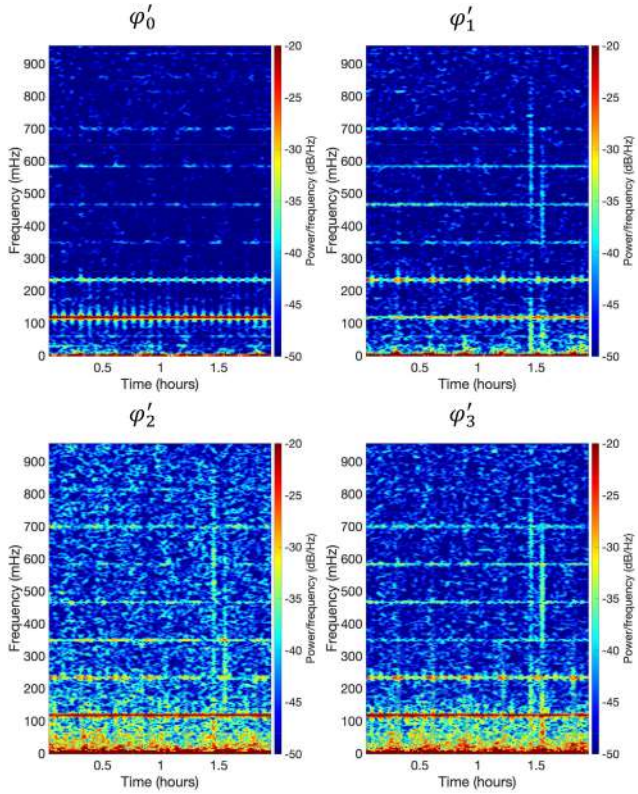

Fig. 6. Spectrograms of the polarization-averaged phase φ'_0 and of the three components of $\vec{\varphi}'$.

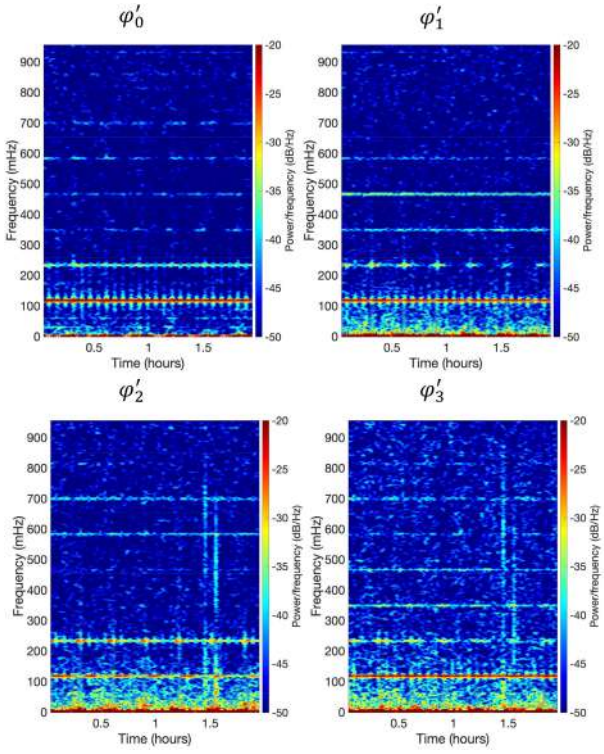

Fig. 7. Same as in Fig. 6, after post-compensation by removal of the average rotation.

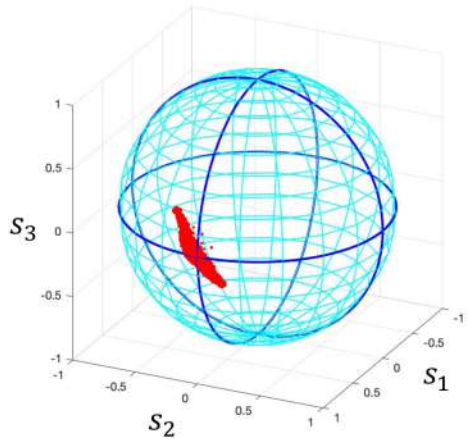

Fig. 8. Scatter plot of the post-compensated output Stokes vector on the Poincaré sphere for an x-polarized input.

post-compensated output Stokes vector on the Poincaré sphere for the data used in Fig. 5. The elongated shape of the data points is a consequence of the 20-minute temporal period of the air conditioning system in the laboratory. Otherwise the scatter plot indicates that the field polarization is stable in the two-hour time interval.

V. Conclusion

We have discussed the sensitivity to environmental perturbations of various quantities that can be extracted from measured transfer matrix. Although the matrix common phase is the most sensitive to time-dependent perturbations when transmit and local-oscillator lasers with sub-hertz line-width are used, we find that the rotation vector that characterizes the unitary part of the transfer matrix is the most sensitive when telecommunication-grade lasers are used, with a line-width in the kilohertz or tens of kilohertz range. Our conclusions our drawn on the basis of real-time data measured on cabled multi-core-fibers (MCF) with nominally uncoupled cores deployed in the city of L'Aquila, Italy, during a field trial in which a FPGA-based real-time transceiver has been operated continuously for approximately two months [3].

Appendix
Expression of the Estimated Rotation Vector $\vec{\varphi}'$

Combining (4), (9) and (12) of the main text we obtain

$$\begin{aligned}&\exp\left(-i\frac{\varphi_0'}{2}\,\mathbf{I}-i\frac{\vec{\varphi}'}{2}\cdot\vec{\sigma}\right)\\&=\exp\left(-i\frac{\varphi_0}{2}\,\mathbf{I}-i\frac{\vec{\varphi}}{2}\cdot\vec{\sigma}\right)\\&\quad\exp\left(-i\frac{\phi_1+\phi_2}{2}\mathbf{I}-i\frac{\phi_1-\phi_2}{2}\,\sigma_1\right),\end{aligned}\tag{26}$$

which is satisfied if (13) holds and

$$\exp\left(-i\frac{\vec{\varphi}'}{2}\cdot\vec{\sigma}\right)=\exp\left(-i\frac{\vec{\varphi}}{2}\cdot\vec{\sigma}\right)\exp\left(-i\frac{\phi}{2}\hat{e}_1\cdot\vec{\sigma}\right),\tag{27}$$

where we used $\phi=\phi_1-\phi_2$ to simplify the notation. Our aim is to find an expression for $\vec{\varphi}'$. Using the expansion

$$\exp\left(-i\vec{\varphi}/2\cdot\vec{\sigma}\right)=\cos(\varphi/2)\mathbf{I}-i\sin(\varphi/2)(\hat{\varphi}\cdot\vec{\sigma}),\tag{28}$$

and the similar one for the second and third exponentials, the identity [5] $(\vec{a}\cdot\vec{\sigma})(\vec{b}\cdot\vec{\sigma})=(\vec{a}\cdot\vec{b})\,\mathbf{I}+i(\vec{a}\times\vec{b})\cdot\vec{\sigma}$ and expanding, we obtain

$$\begin{aligned}&\cos(\varphi'/2)\mathbf{I}-i\sin(\varphi'/2)(\hat{\varphi}'\cdot\vec{\sigma})\\&=\big[\cos(\varphi/2)\cos(\phi/2)\\&\quad-\sin(\varphi/2)\sin(\phi/2)(\hat{\varphi}\cdot\hat{e}_1)\big]\mathbf{I}\\&\quad-i\big[\sin(\varphi/2)\cos(\phi/2)\hat{\varphi}\\&\quad+\cos(\varphi/2)\sin(\phi/2)\hat{e}_1\\&\quad+\sin(\varphi/2)\sin(\phi/2)(\hat{\varphi}\times\hat{e}_1)\big]\cdot\vec{\sigma}.\end{aligned}\tag{29}$$

The identity of the projections over $\vec{\sigma}$ gives

$$\begin{aligned}\hat{\varphi}'\sin(\varphi'/2)=\;&\sin(\varphi/2)\cos(\phi/2)\hat{\varphi}\\&+\cos(\varphi/2)\sin(\phi/2)\hat{e}_1\\&+2\sin(\varphi/2)\sin(\phi/2)(\hat{\varphi}\times\hat{e}_1)\end{aligned}\tag{30}$$

Taking the modulus of both sides of (30) we obtain

$$\begin{aligned}\sin^2(\varphi'/2)=\;&\sin^2(\varphi/2)\cos^2(\phi/2)\\&+\cos^2(\varphi/2)\sin^2(\phi/2)\\&+\sin^2(\varphi/2)\sin^2(\phi/2)[1-(\hat{\varphi}\cdot\hat{e}_1)^2]\\&+2\sin(\varphi/2)\cos(\phi/2)\\&\cos(\varphi/2)\sin(\phi/2)\hat{\varphi}\cdot\hat{e}_1.\end{aligned}\tag{31}$$

Equation (31) can be readily solved for φ' and its result, entered into (30), gives an explicit expression of $\hat{\varphi}'$, thus completing the determination of $\vec{\varphi}'=\varphi'\hat{\varphi}'$. A more transparent expression can however be obtained assuming ϕ small, and using the expansions

$$\varphi'=\varphi'^{(0)}+\varphi'^{(1)}\phi+\ldots,\tag{32}$$

$$\hat{\varphi}'=\hat{\varphi}'^{(0)}+\hat{\varphi}'^{(1)}\phi+\ldots,\tag{33}$$

Inserting (32) into (31) and retaining only the terms to first order in ϕ we obtain

$$\begin{aligned}&\sin^2(\varphi'^{(0)}/2)+\sin(\varphi'^{(0)}/2)\cos(\varphi'^{(0)}/2)\varphi'^{(1)}\phi\\&=\sin^2(\varphi/2)+\sin(\varphi/2)\cos(\varphi/2)(\hat{\varphi}\cdot\hat{e}_1)\phi,\end{aligned}\tag{34}$$

which gives, for $0\leqslant\varphi\leqslant\pi$,

$$\varphi'^{(0)}=\varphi,\tag{35}$$

$$\varphi'^{(1)}=\hat{\varphi}\cdot\hat{e}_1,\tag{36}$$

so that

$$\varphi'=\varphi+(\hat{\varphi}\cdot\hat{e}_1)\phi.\tag{37}$$

Inserting then (32) into (31) and again retaining only the terms of first order in ϕ we obtain

$$(\hat{\varphi}'^{(0)} + \hat{\varphi}'^{(1)}\phi)\sin(\varphi'^{(0)}/2) + \hat{\varphi}'^{(0)}\cos(\varphi'^{(0)}/2)\varphi'^{(1)}\phi/2 = \sin(\varphi/2)\hat{\varphi} + [(1/2)\cos(\varphi/2)\,\hat{e}_1 + (1/2)\sin(\varphi/2)\,(\hat{\varphi}\times\hat{e}_1)]\phi. \tag{38}$$

so that

$$\hat{\varphi}'^{(0)} = \hat{\varphi}, \tag{39}$$

and using (35) and (36) we obtain

$$\begin{aligned}\sin(\varphi/2)\hat{\varphi}'^{(1)} = &-\hat{\varphi}\cos(\varphi/2)\hat{\varphi}\cdot\hat{e}_1/2 \\ &+ (1/2)\cos(\varphi/2)\hat{e}_1 \\ &+ (1/2)\sin(\varphi/2)(\hat{\varphi}\times\hat{e}_1).\end{aligned} \tag{40}$$

that is

$$\begin{aligned}\hat{\varphi}'^{(1)} = &-\hat{\varphi}\cot(\varphi/2)\hat{\varphi}\cdot\hat{e}_1/2 + (1/2)\cos(\varphi/2)\hat{e}_1 \\ &+ (1/2)(\hat{\varphi}\times\hat{e}_1),\end{aligned} \tag{41}$$

and consequently

$$\begin{aligned}\hat{\varphi}' = \hat{\varphi} + \big[&(1/2)(\hat{e}_1 - \hat{\varphi}\cdot\hat{e}_1\,\hat{\varphi})\cot(\varphi/2)\hat{e}_1 \\ &+ (1/2)(\hat{\varphi}\times\hat{e}_1)\big]\phi.\end{aligned} \tag{42}$$

Using now that $\vec{\varphi}' = \varphi'\hat{\varphi}'$, retaining in the product only the first order terms in ϕ so that

$$\vec{\varphi} \simeq \varphi^{(0)}\hat{\varphi}'^{(0)} + \left(\varphi^{(0)}\hat{\varphi}'^{(1)} + \varphi^{(1)}\hat{\varphi}'^{(0)}\right)\phi, \tag{43}$$

and using (35), (36), (39) and (41), we obtain

$$\begin{aligned}\vec{\varphi}' = \vec{\varphi} + \big\{&(\hat{\varphi}\cdot\hat{e}_1)\,\hat{\varphi} + [\hat{e}_1 - (\hat{\varphi}\cdot\hat{e}_1)\,\hat{\varphi}]\,(\varphi/2)\cot(\varphi/2) \\ &+ (1/2)(\vec{\varphi}\times\hat{e}_1)\big\}\phi.\end{aligned} \tag{44}$$

Inserting back the definition $\phi = \phi_1 - \phi_2$, this equation becomes (14)–(18) of the main text.

REFERENCES

[1] Z. Zhan et al., "Optical polarization–based seismic and water wave sensing on transoceanic cables," *Science*, vol. 371, no. 6532, pp. 931–936, 2021. [Online]. Available: https://science.sciencemag.org/content/371/6532/931

[2] A. Mecozzi, M. Cantono, J. C. Castellanos, V. Kamalov, R. Muller, and Z. Zhan, "Polarization sensing using submarine optical cables," *Optica*, vol. 8, no. 6, pp. 788–795, Jun. 2021. [Online]. Available: http://www.osapublishing.org/optica/abstract.cfm?URI=optica-8-6-788

[3] T. Hayashi et al., "Field-deployed multi-core fiber testbed," in *Proc. IEEE 24th OptoElectron. Commun. Conf. Int. Conf. Photon. Switching Comput.*, 2019, pp. 1–3.

[4] A. Mecozzi et al., "Use of optical coherent detection for environmental sensing," in *Proc. Eur. Conf. Opt. Commun.*, 2022, Paper Tu3D.1. [Online]. Available: https://opg.optica.org/abstract.cfm?URI=ECEOC-2022-Tu3D.1

[5] J. P. Gordon and H. Kogelnik, "PMD fundamentals: Polarization mode dispersion in optical fibers," *Proc. Nat. Acad. Sci.*, vol. 97, no. 9, pp. 4541–4550, 2000. [Online]. Available: https://www.pnas.org/content/97/9/4541

[6] A. Mecozzi and M. Shtaif, "Signal-to-noise-ratio degradation caused by polarization-dependent loss and the effect of dynamic gain equalization," *J. Lightw. Technol.*, vol. 22, no. 8, pp. 1856–1871, Aug. 2004. [Online]. Available: http://opg.optica.org/jlt/abstract.cfm?URI=jlt-22-8-1856

[7] S. J. Savory, "Digital coherent optical receivers: Algorithms and subsystems," *IEEE J. Sel. Topics Quantum Electron.*, vol. 16, no. 5, pp. 1164–1179, Sep./Oct. 2010.

[8] M. Karlsson and E Agrell, "Spectrally efficient four-dimensional modulation," in *Proc. Opt. Fiber Commun. Conf.*, 2012, Paper OTu2C.1. [Online]. Available: http://opg.optica.org/abstract.cfm?URI=OFC-2012-OTu2C.1

[9] M. Mazur et al., "Real-time MIMO transmission over field-deployed coupled-core multi-core fibers," in *Proc. Opt. Fiber Commun. Conf.*, 2022, Paper Th4B.8. [Online]. Available: http://opg.optica.org/abstract.cfm?URI=OFC-2022-Th4B.8

[10] A. Mecozzi and M. Shtaif, "The statistics of polarization-dependent loss in optical communication systems," *IEEE Photon. Technol. Lett.*, vol. 14, no. 3, pp. 313–315, Mar. 2002.

Open Access funding provided by 'Università degli Studi dell'Aquila' within the CRUI CARE Agreement